Focused Circular Piston

Axial field ($\rho = 0$):

$$p_w(0,z) = -ik\rho_0 c_0 u_0 \frac{e^{ikz}}{z} \int_0^a e^{\frac{ik}{2}\left(\frac{1}{z}-\frac{1}{d}\right)\rho_0^2} \rho_0 d\rho_0$$

$$\int e^{\alpha x^2} x\, dx = \frac{1}{2\alpha} e^{\alpha x^2}$$

$$p_w(0,z) = \rho_0 c_0 u_0 \frac{e^{ikz}}{1-z/d} \left[1 - e^{i\frac{ka^2}{2z}(1-z/d)}\right] \qquad (1)$$

$$= -iz\rho_0 c_0 u_0 \frac{\sin\frac{G}{2}(d/z-1)}{1-z/d} \cdot e^{ikz} e^{i\frac{G}{2}(d/z-1)}, \quad G = \frac{ka^2}{2d}$$

$$\to -iz\rho_0 c_0 u_0 \sin\frac{z_0}{2z}\, e^{ikz + iz_0/2z}, \quad d \to \infty \ \checkmark$$

$$\frac{|p_w(0,z)|}{\rho_0 c_0 u_0} = 2\left|\frac{\sin\frac{G}{2}(d/z-1)}{1-z/d}\right|$$

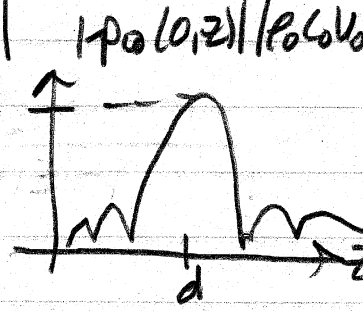

From (1),

$$\lim_{z\to d} \frac{p_w(0,z)}{\rho_0 c_0 u_0} = \lim \frac{e^{ikz}}{1-z/d} \cdot \left[-\frac{ika^2}{2z}(1-z/d) + \cdots\right]$$

$$= -iG e^{ikd} \ \checkmark$$

Measurements of harmonic generation in a focused finite-amplitude sound beam

Michalakis A. Averkiou[a] and Mark F. Hamilton
Department of Mechanical Engineering, The University of Texas at Austin, Austin, Texas 78712-1063

(Received 24 August 1994; revised 1 May 1995; accepted 31 May 1995)

Measurements of harmonic generation in the sound field radiated by a focused circular piston source are compared with numerical calculations based on the nonlinear parabolic wave equation. The large dynamic range and high spatial resolution of the measurements enable precise comparisons to be made with the theoretical predictions. © *1995 Acoustical Society of America.*

PACS numbers: 43.25.Cb

INTRODUCTION

The purpose of this article is to report precise measurements of harmonic generation in the field of a focused circular piston source that radiates finite-amplitude sound in water. The measurements are compared with numerical solutions of the KZK nonlinear parabolic wave equation.[1] Our work is therefore similar to that reported in a recent article by Baker.[2] The large dynamic range and high spatial resolution of the measurements presented here permit detailed comparisons to be made with theory. Additionally, measured beam patterns are shown at a greater number of distances than has been reported previously in the literature. Finally, the measurements reveal very clearly earlier theoretical predictions[3] of the shift toward the axis in the positions of the nonlinearly generated sidelobes in the focal plane.

I. THEORY

Our theoretical predictions are based on the KZK equation. The equation is solved numerically with the version of the spectral code described by Naze Tjøtta *et al.*[4] The sound pressure is expanded in a Fourier series, and the resulting set of coupled equations for the spectral amplitudes is solved with finite difference methods. In the parabolic approximation, the appropriate source condition in the plane $z=0$ is[4,5]

$$p=p_0 \sin(\omega_0 t+\omega_0 r^2/2c_0 d)H(1-r/a), \quad z=0, \qquad (1)$$

where a is the radius and d the focal length of the source, ω_0 is the angular frequency, p_0 the peak sound pressure at the source, c_0 the sound speed, r the distance from the z axis, and H the unit step function: $H(x)=0$ for $x<0$ and $H(x)=1$ for $x\geqslant 0$.

Three dimensionless parameters are used to characterize the field radiated by the focused source. Each is normalized by the focal length d:

$$G=z_0/d, \quad A=\alpha_0 d, \quad N=d/\bar{z}. \qquad (2)$$

The focusing gain G, expressed in terms of the Rayleigh distance $z_0=\omega_0 a^2/2c_0$, is the peak value of p/p_0 at the geometric focus $(r,z)=(0,d)$ in the absence of absorption and nonlinearity. The absorption parameter A is proportional to the small signal attenuation coefficient α_0 at frequency ω_0 for a thermoviscous fluid. The nonlinearity parameter N is inversely proportional to the plane wave shock formation distance $\bar{z}=\rho_0 c_0^3/\beta\omega_0 p_0$, where β is the coefficient of nonlinearity, and ρ_0 is the ambient density of the fluid.

II. EXPERIMENT

Our focused source was manufactured by Harisonic and consists of a single PZT element, with one side cut to form a spherical concave surface. The source has effective radius $a=18.8$ mm and focal length $d=160$ mm, and it was driven at 2.25 MHz. With the measured sound speed given by $c_0=1486$ m/s, the focusing gain is $G=10.6$. To simulate CW operation we used tone bursts with 40–50 cycles. Our receiver was a bilaminar Marconi PVDF membrane hydrophone, the active element of which has a diameter of 1 mm and thickness of 25 μm. The upper cutoff frequency of the hydrophone is above 20 MHz. A Blackman–Harris window was applied to the captured waveforms to suppress leakage, and an FFT was performed on the windowed waveform to obtain harmonic amplitudes for the propagation curves and beam patterns. The Sony/Tektronix RTD 710 digitizer that was used to capture waveforms has 10-bit amplitude resolution, which corresponds to dynamic range of 60 dB. Repeated averaging of the captured waveforms, typically 1024 times, further improved the dynamic range. The experiments were performed in the ultrasonics tank facility described previously by TenCate.[6] The spatial resolution of the positioning apparatus is approximately 20 μm.

To determine the effective source radius and focal length cited in the previous paragraph, we compared small signal measurements with the axial theory presented by Lucas and Muir.[5] Their solution was derived from the lossless and linear form of the KZK equation, and it is equivalent to the solution of the Helmholtz equation in the Fresnel approximation. The source parameters were determined by matching the predicted locations of the axial nulls immediately before ($z=100$ mm) and after ($z=398$ mm) the focus, as well as the location of the peak pressure in the focal region ($z=150$

[a]Present address: Applied Physics Laboratory, University of Washington, Seattle, WA 98105.

 0001-4966/95/98(6)/3439/4/$6.00

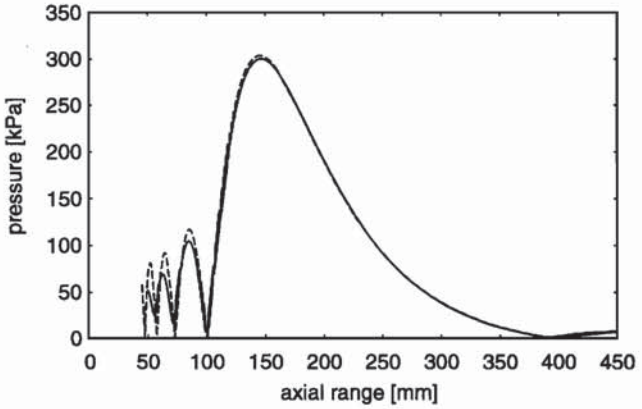

FIG. 1. Comparison of small signal measurements (solid line) and linear theory (dashed line) for the pressure amplitude along the axis of the beam.

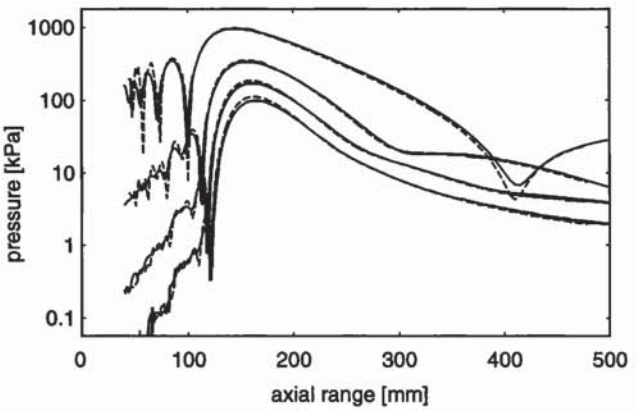

FIG. 2. Comparison of experiment (solid lines) and theory (dashed lines) for the pressure amplitudes of the lowest four harmonic components (fundamental through fourth harmonic in top to bottom order) along the axis of the beam.

mm), with the corresponding measurements. Although the parameter values determined in this way are close to those which were requested from the manufacturer (the latter being $a=0.75$ in.$=19.1$ mm and $d=6$ in.$=152$ mm), the small differences nevertheless introduce observable discrepancies between theory and experiment. The small signal measurements are shown as the solid line in Fig. 1, and the dashed line is linear theory[5] evaluated with the adjusted parameters. The adjusted parameters were used to obtain the numerical solutions presented in Sec. III.

III. RESULTS

Measurements of the sound field radiated at finite amplitude are compared in this section with numerical predictions obtained from the KZK equation for the source condition in Eq. (1).

Measured axial propagation curves for the first four harmonics in the focused beam are shown as solid lines in Fig. 2 (the uppermost curve is for the fundamental component, the next is for the second harmonic, and so on). The numerical calculations (dashed lines) were obtained with $A=0.025$ and $N=0.212$, and with 12 harmonics retained in the Fourier series expansion. To determine the absorption parameter we began with the nominal expression for attenuation in water at room temperature[7] ($\alpha_0/f_0^2=25\times10^{-15}$ Np/m/Hz^2, where $f_0=\omega_0/2\pi$), which yields $A=0.020$ for $f_0=2.25$ MHz. An estimate of the nonlinearity parameter was based on direct measurement of the fundamental component in the prefocal region and use of linear theory[5] to estimate p_0, which yielded $N=0.217$. The values of A and N were then adjusted to optimize agreement between theory and experiment, which resulted in the values $A=0.025$ and $N=0.212$ stated above and used to calculate the dashed lines in Fig. 2.

Good overall agreement is observed throughout the propagation curves. Results are not presented closer to the source than about 50 mm, where the parabolic approximation eventually breaks down. (See the discussion by Naze Tjøtta *et al.*[4] on quantitative estimates of regions where the parabolic approximation is expected to be valid.) Note especially

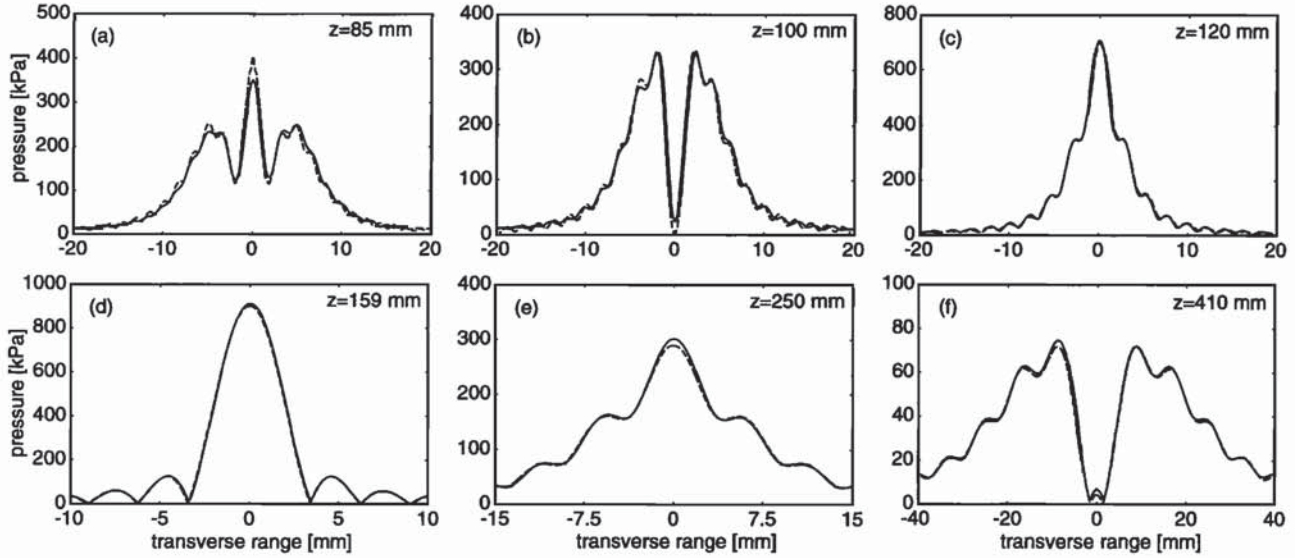

FIG. 3. Comparison of experiment (solid lines) and theory (dashed lines) for the transverse pressure distribution of the fundamental component as a function of distance from the source.

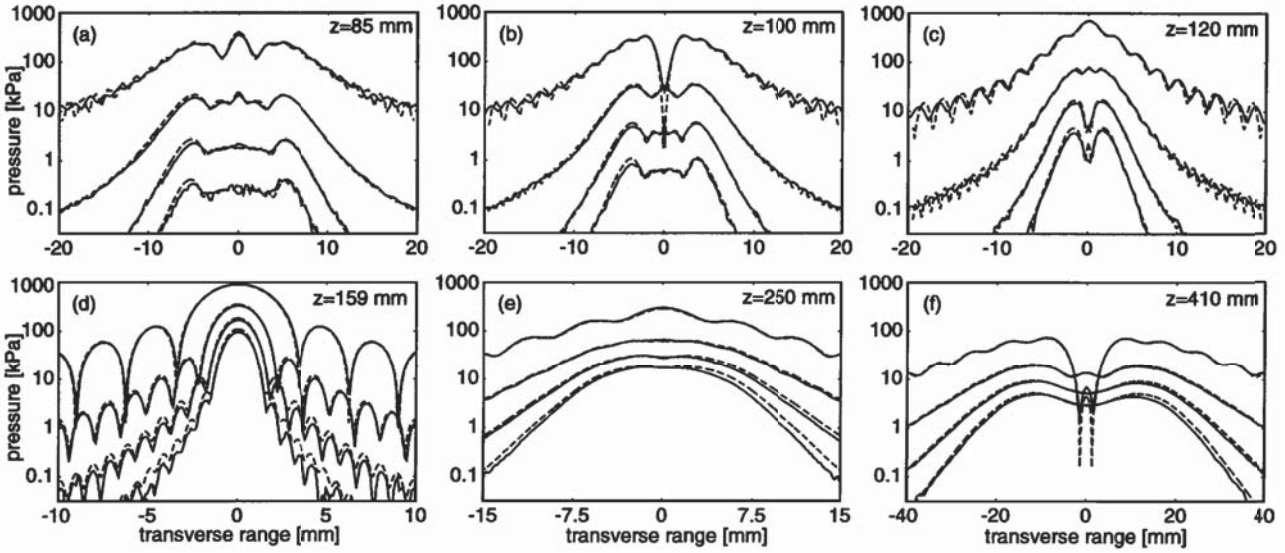

FIG. 4. Comparison of experiment (solid lines) and theory (dashed lines) for the transverse pressure distributions of the lowest four harmonic components (fundamental through fourth harmonic in top to bottom order) as functions of distance from the source.

the good agreement between theory and experiment at distances 50–100 mm from the source, i.e., before the last prefocal null in the propagation curve for the primary wave. The locations of the last prefocal nulls in all four harmonic propagation curves are predicted quite accurately by theory.

In Fig. 3 are shown transverse amplitude distributions for the fundamental component. The axial locations of the beam patterns in Fig. 3(a) and (b) correspond to the last prefocal maximum and minimum, respectively, in the propagation curve for the fundamental component. At the geometric focus, shown in Fig. 3(d), the familiar Bessel directivity is obtained. Beyond the focus the sidelobe structure disappears as the beam diverges. The last beam pattern, in Fig. 3(f), was measured at the location seen where the postfocal axial minimum occurs in the propagation curve for the fundamental component (recall Fig. 2).

Beam patterns for the first four harmonic components, at the same locations as in Fig. 3, are presented in Fig. 4 (now on a logarithmic amplitude scale). As in Fig. 2, the uppermost curves are for the fundamental component, the next are for the second harmonic, etc. Excellent agreement is again obtained between theory and experiment. In particular, the sidelobe structure of all four components is predicted very accurately in the focal plane, particularly the "fingers" (i.e., additional sidelobes[8,9]) in the second and higher harmonic patterns. Note the inward shift in the positions of the sidelobes in the second and higher harmonic beam patterns, relative to the sidelobe locations in the primary wave beam pattern. This phenomenon was predicted in an earlier numerical investigation of focused beams,[3] and Fig. 4(d) provides clear experimental confirmation.

Two-dimensional scans in the focal plane produced the primary and second harmonic field measurements shown in Fig. 5. The measurements illustrate the axial symmetry of the beam and the generation of the additional sidelobes in the second harmonic field.

IV. CONCLUSION

The measurements presented above provide a detailed portrayal of harmonic generation in the sound field of a focused circular piston with uniform amplitude shading. The large dynamic range and high spatial resolution of the measurements enabled precise comparisons to be made with numerical calculations based on the KZK nonlinear parabolic wave equation. Most notably, the theoretically predicted inward shift of sidelobes in the nonlinearly generated harmonic

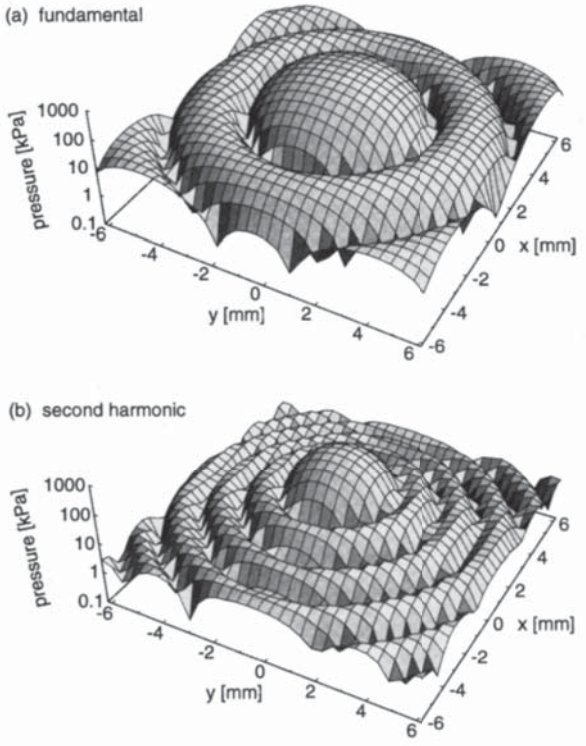

FIG. 5. Measured pressure amplitudes of the fundamental and second harmonic components in the focal plane.

beam patterns[3] was clearly revealed. To facilitate comparison with other theoretical models, the same measurements are presented elsewhere,[10] without the predictions based on the KZK equation.

ACKNOWLEDGMENTS

This work was supported by the David and Lucile Packard Foundation Fellowship for Science and Engineering, and by the Office of Naval Research. Preliminary support from the National Science Foundation and the Texas Advanced Research Program for construction of the ultrasonics tank facility is gratefully acknowledged. Partial support from the National Institutes of Health is also acknowledged.

[1] N. S. Bakhvalov, Ya. M. Zhileikin, and E. A. Zabolotskaya, *Nonlinear Theory of Sound Beams* (American Institute of Physics, New York, 1987).
[2] A. C. Baker, "Nonlinear pressure fields due to focused circular apertures," J. Acoust. Soc. Am. **91**, 713–717 (1992).
[3] T. S. Hart and M. F. Hamilton, "Nonlinear effects in focused sound beams," J. Acoust. Soc. Am. **84**, 1488–1496 (1988).
[4] J. Naze Tjøtta, S. Tjøtta, and E. H. Vefring, "Effects of focusing on the nonlinear interaction between two collinear finite amplitude sound beams," J. Acoust. Soc. Am. **89**, 1017–1027 (1991).
[5] B. G. Lucas and T. G. Muir, "The field of a focusing source," J. Acoust. Soc. Am. **72**, 1289–1296 (1982).
[6] J. A. TenCate, "An experimental investigation of the nonlinear pressure field produced by a plane circular piston," J. Acoust. Soc. Am. **94**, 1084–1089 (1993).
[7] L. E. Kinsler, A. R. Frey, A. B. Coppens, and J. V. Sanders, *Fundamentals of Acoustics* (Wiley, New York, 1982), 3rd ed., p. 148.
[8] J. Berntsen, J. Naze Tjøtta, and S. Tjøtta, "Nearfield of a large acoustic transducer. Part IV: Second harmonic and sum frequency radiation," J. Acoust. Soc. Am. **75**, 1383–1391 (1984).
[9] M. F. Hamilton, J. Naze Tjøtta, and S. Tjøtta, "Nonlinear effects in the farfield of a directive sound source," J. Acoust Soc. Am. **78**, 202–216 (1985).
[10] M. A. Averkiou, "Experimental investigation of propagation and reflection phenomena in finite-amplitude sound beams," Ph.D. dissertation, The University of Texas at Austin (1994), Appendix B.